AGU PUBLICATIONS

Geophysical Research Letters

RESEARCH LETTER
10.1002/2015GL067372

Key Points:
- Multiphase mixing in crystal-rich magmas is often observed but poorly understood
- A multiphase mixing index is used to quantify and predict crystal mixing
- Local crystal mixing shows a remarkable diversity of simultaneous scales

Supporting Information:
- Table S1 and caption for Movie S1
- Movie S1

Correspondence to:
G. W. Bergantz,
bergantz@uw.edu

Citation:
Schleicher, J. M., G. W. Bergantz, R. E. Breidenthal, and A. Burgisser (2016), Time scales of crystal mixing in magma mushes, *Geophys. Res. Lett.*, *43*, doi:10.1002/2015GL067372.

Received 9 DEC 2015
Accepted 5 FEB 2016
Accepted article online 17 FEB 2016

Time scales of crystal mixing in magma mushes

Jillian M. Schleicher[1], George W. Bergantz[1], Robert E. Breidenthal[2], and Alain Burgisser[3]

[1]Department of Earth and Space Sciences, University of Washington, Seattle, Washington, USA, [2]William E. Boeing Department of Aeronautics and Astronautics, College of Engineering, University of Washington, Seattle, Washington, USA, [3]Institut des Sciences de la Terre, CNRS–IRD, Université de Savoie, Campus Scientifique, Le Bourget du Lac, France

Abstract Magma mixing is widely recognized as a means of producing compositional diversity and preconditioning magmas for eruption. However, the processes and associated time scales that produce the commonly observed expressions of magma mixing are poorly understood, especially under crystal-rich conditions. Here we introduce and exemplify a parameterized method to predict the characteristic mixing time of crystals in a crystal-rich magma mush that is subject to open-system reintrusion events. Our approach includes novel numerical simulations that resolve multiphase particle-fluid interactions. It also quantifies the crystal mixing by calculating both the local and system-wide progressive loss of the spatial correlation of individual crystals throughout the mixing region. Both inertial and viscous time scales for bulk mixing are introduced. Estimated mixing times are compared to natural examples and the time for basaltic mush systems to become well mixed can be on the order of 10 days.

1. Introduction

The compositional diversity and eruptive behavior of volcanic systems are often attributed to magma mixing. An obstacle to understanding the mixing processes is that the crystal cargo is complex, as expressed by crystal textures and chemical zoning [*Charlier et al.*, 2007; *Davidson et al.*, 2005, 2007; *Ginibre et al.*, 2007; *Martin et al.*, 2010; *Wallace and Bergantz*, 2005]. This complexity arises from crystal and melt transfer during repeated open-system reintrusion events [*Kahl et al.*, 2011; *Perugini and Poli*, 2012; *Ruprecht et al.*, 2012], the remobilization of cumulates [*Klemetti and Clynne*, 2014; *Passmore et al.*, 2012], and the mechanical entrainment of antecrysts from the magma chamber walls and floor [*Davidson et al.*, 2007]. Because of this complexity, identifying the time scales over which crystal-rich magmas transition from one spatial distribution and thermodynamic state to another by mixing has been elusive.

Numerous schemes have been employed to quantify mixing in magmas and the Earth's mantle. Mixing has often been described in terms of the evolution of Eulerian scalar field variables, as implemented in continuum numerical simulations, often including passive tracers [*Oldenburg et al.*, 1989; *Tackley and King*, 2003; *van Keken and Zhong*, 1999], analog laboratory experiments [*Jellinek et al.*, 1999; *Laumonier et al.*, 2014; *Sato and Sato*, 2009; *Turner and Campbell*, 1986], or a mixture of dynamic and kinematic elements in a reduced system amenable to chaotic analysis (Lyapunov exponents, chaotic advection, and twist maps) [*Bergantz*, 2000; *Coltice and Schmalzl*, 2006; *Farnetani and Samuel*, 2003; *Ferrachat and Ricard*, 1998; *Kellogg and Turcotte*, 1990; *Perugini et al.*, 2012]. However, it is an open question if these methods can be applied to multiphase systems such as crystal-rich, non-Brownian multiphase mixtures, as they can exhibit nonaffine deformation and nonlocal rheology [*Bouzid et al.*, 2013; *Lemaître et al.*, 2009].

The mixing, or dispersion, of granular mixtures differs from that of pure fluids. (In this study we use the terms crystals and particles interchangeably.) The distribution of non-Brownian particles in a multiphase mixing system reflects the competition between flow-induced advection and particle segregation, the latter a process without parallel in single-phase fluids. Processes intended to produce multiphase mixing may instead cause the granular fraction to separate or unmix because of particle properties such as density or size; in non-Brownian systems this produces metastable nonuniform particle distributions. Even in dilute, low-Reynolds number flow, particles can migrate across streamlines [*Guazzelli and Morris*, 2012], and particles of low ($<<1$) but different Stokes numbers can be locally separated [*Bec et al.*, 2005]. In dense viscous suspensions, lubrication forces can make it difficult to initiate the phase-relative motion required to mix a suspension [*Mutabaruka et al.*, 2014]. Hence, there is no a priori reason to expect that the mixing of crystals, being of finite size and mass, can be modeled as tracers, nor that simply quantifying the global strain rate within the mixing domain provides a reliable metric of particle trajectory and hence the progress of crystal mixing.

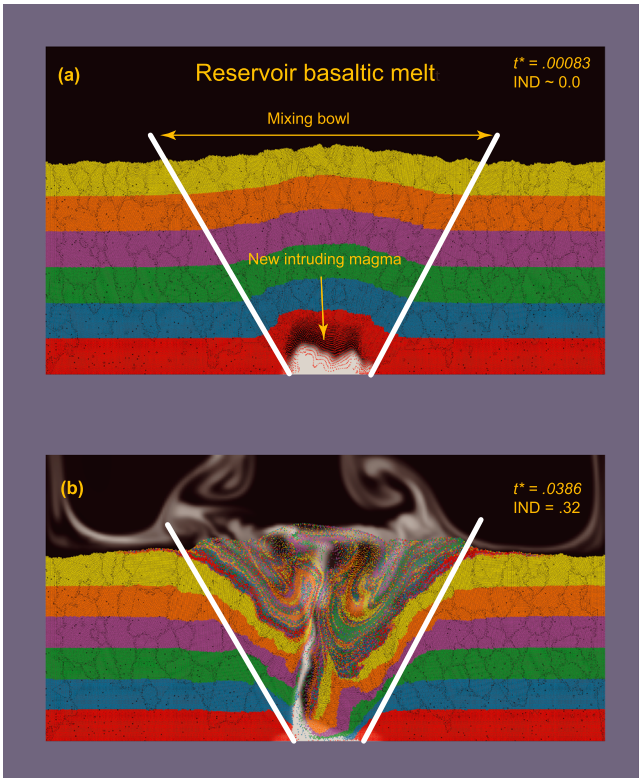

Figure 1. Two time steps taken from the simulation of an open-system event in basaltic mush. (a) An olivine mush with about 40% porosity is shown in side view. Resident basaltic liquid is colored black, and new magma, colored white, intrudes from below. The interplay between pore pressure and crystal contact properties induces a viscoplastic response that creates a mixing bowl and (b) causes overturn, subsequently mixing crystals and melts.

2. A Mixing Paradigm for Crystal-Rich Magma Mushes

The most significant difficulty in understanding crystal-rich magma mixing is the absence of real-time observational constraints on the volumes and mechanisms involved. However, recent two-dimensional numerical modeling of open-system events in crystal-rich magma mushes using discrete element, computational fluid dynamics modeling (DEM-CFD) provides a template for quantifying mixing, and we employ that template here to further quantify crystal-rich mixing [*Bergantz et al.*, 2015]. The DEM-CFD method explicitly considers frictional, collisional, translational, buoyant, lubrication, and viscous particle-particle-fluid coupling at the crystal scale, and the mechanical coupling between the resident and intruding liquids and the crystal mush.

Specifically, *Bergantz et al.* [2015] demonstrated that at the start of a reintrusion event, a crystal mush at random close packing can respond initially as a viscoplastic material when intruded from below by a pure melt. The propagation of granular-fluid stresses associated with a new intrusion creates localized conjugate failure modes or soft faults, and these delimit a fluidized region called the mixing bowl. Figure 1a shows the essential features of the mixing bowl, which approximates the maximum available volume of the crystal pile available for mixing. Following the initial viscoplastic response, portions of the mixing bowl can become fluidized and participate in time-dependent overturn and mixing as shown in Figure 1b and in the supporting information Video S1.

For crystal mixing to occur within a crystal-rich mush, intruding melt must fluidize settled crystals by locally decreasing their packing. At a minimum this requires that the intruding melt enters the crystal mush at a sufficient rate to overcome the weight of the crystals in the bed. This rate is known as the minimum fluidization velocity, U_{mf}. The U_{mf} of a system is typically calculated using the Ergun equation (equation (1)), with the condition that the drag force on the particles from the injected fluid equals the weight of the bed (equation (4)):

$$\frac{-\Delta P}{H_0} = \alpha U_0 + \beta U_0^2 \tag{1}$$

$$\alpha = 150\frac{(1-\varepsilon_f)^2}{\varepsilon_f^3}\frac{\mu_f}{d_p^2} \tag{2}$$

$$\beta = 1.75\frac{(1-\varepsilon_f)}{\varepsilon_f^3}\frac{\rho_f}{d_p} \tag{3}$$

$$\left(1-\varepsilon_f\right)\left(\rho_p-\rho_f\right)g = \alpha U_{\mathrm{mf}} + \beta U_{\mathrm{mf}}^2. \tag{4}$$

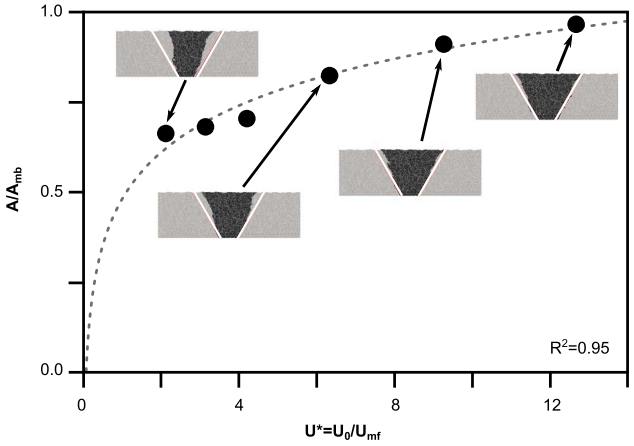

Figure 2. The volume (area, for our 2-D simulations) of magma that is mobilized by the intruding crystal-free magma depends on the mass flux of the intrusion. Data points represent the area fraction of mobilized crystals, A, to mixing bowl crystals, A_{mb}, and are fit with a logarithmic function (dashed line). A logarithmic fit is used to give an area fraction of zero as the mass flux goes to zero. Inset images display the mobilized crystals for four U^* values. Grey regions are stationary crystals, black regions are mobilized crystals, and white lines delimit the mixing bowl with 60° angles from the horizontal on either side of the intrusion.

Here ΔP is the fluid pressure drop across a particle bed of height H_0, U_0 is the superficial velocity entering the base of the system, ε_f is the fluid fraction (porosity), μ_f is the dynamic viscosity of the fluid, ρ_f is the fluid density, d_p is the particle diameter, ρ_p is the particle density, and g is the magnitude of gravitational acceleration. This calculation only considers the pressure drop across the bed in a mixture of particles and fluid and does not consider the effect of granular forces such as contact friction or geometrical jamming that will impact the true minimum velocity for fluidization.

Following *Bergantz et al*. [2015], new melt intrudes only a portion of the base of the lateral extent of the mush in our simulations. The mixing bowl (Figure 1) is tapered and opens upward; therefore, the Ergun equation must be modified. The modified calculation of U_{mf} accounts for the small injection region relative to the domain size [*Cui et al*., 2014]:

$$\frac{1}{2}\,\theta\beta\, l_w^2 \ln\left(\frac{2H_0}{l_w}\right) U_{mf}^2 + \theta\alpha l_w \left(H_0 - \frac{l_w}{2}\right) U_{mf} = \left(l_w + H_0 \tan\theta\right) H_0 \left(\rho_p - \rho_f\right) g \left(1 - \varepsilon_f\right), \tag{5}$$

where θ is the angle from the vertical at the edges of the fluidized region (mixing bowl) and l_w is the width of the intrusion inlet. This modified equation defines a dimensionless velocity, $U^* = U_0/U_{mf}$, for the system. In the case that $U^* < 1$, melt enters the domain at a rate lower than U_{mf}, moving through the mush as porous flow. When $U^* > 1$, the melt enters at a rate exceeding U_{mf} and fluidizes the crystals, as is the case in the presented simulations.

3. Calculating Open-System Mixing in Crystal Mush

3.1. Quantifying the Mixing of Discrete Phases

The quantification of particle mixing has obvious industrial applications, and at least 40 different schemes have been proposed to quantify the mixing of solid particles [*Poux et al*., 1991]. In almost all cases, a single metric was sought that gives a measure of the goodness of mixing throughout the entire active region. The requirements for a general index of mixing should [*Doucet et al*., 2008] (1) satisfy sample size, frame invariance, and ergodicity requirements; (2) have a connection to the spatial coordinates to identify the major and minor directions of the progress of mixing; (3) have grid independence; and (4) resolve both weak and strong mixing. Weak mixing or "color mixing" is defined as a process where there is a progressive loss of the spatial correlation of the mixing constituents from an initial distribution as mechanically neutral, colored particles. Strong mixing refers to the additional loss of spatial correlation of properties usually leading to segregation such as size, density, or shape. It follows that any system mixed in the strong sense is also mixed in the weak sense.

3.2. The Initial Neighbor Distance Mixing Index

To quantify the progress of crystal mixing in a magma mush, we employ the initial neighbor distance (IND) mixing index [*Deen et al*., 2010]. The IND varies from an initial condition value of zero, to a maximum of unity, which is the random, well-mixed state. The IND satisfies the requirements listed in 3.1 above and, unlike the Lacey Index of mixing used by *Bergantz et al*. [2015], does not depend on grid size. In our application of the

IND, the requirement of ergodicity is automatically satisfied because we evaluate all the particles that are available to be mixed (Figure 2).

The IND mixing index is obtained by recording the distances between initially neighboring particles at the start of mixing and summing them at every subsequent time step as the particles are dispersed. This is done for all initially active particles in the mixing domain. Because the kinematics of fluidized magma mushes can be complex, particles move apart and together, which produces noise in the initial neighbor distance time series. To reduce this noise, a second time series is created consisting of the distance between each particle and a random particle. The final IND is created from the ratio of the summed initial neighbor distances:

$$\mathrm{IND} = \frac{\sum_{N_{\mathrm{part}}} r_{ij} - d_p}{\sum_{N_{\mathrm{part}}} r_{ik} - d_p}. \tag{6}$$

Here N_{part} is the number of particles involved in the mixing calculation (see Figure 2), r_{ij} is the distance between particle i and its initial nearest neighbor particle j, and r_{ik} is the distance between particle i and its random initially paired particle k.

4. Characteristic Crystal Mixing Time Calculation

4.1. Dimensionless Time Scale and Mixing Time Calculation

The choice of a characteristic time scale for dense suspension mixing is not obvious because it is controlled by a large number of degrees of freedom reflecting both fluid and granular modes of mechanical coupling and dissipation [*Marzougui et al*., 2015; *Ness and Sun*, 2015]. To first order, mixing in our simulations results from vertical transport in the central chimney and large-scale overturns within the fluidized region. The proposed scaling properties treat the suspension as a single-phase mixture, the Reynolds number (*Re*) of which is

$$Re = \frac{\rho_{\mathrm{mix}} U_0 \sqrt{A}/2}{\mu_{\mathrm{mix}}}, \tag{7}$$

where ρ_{mix} is the mixture density ($\rho_{\mathrm{mix}} = \varepsilon_f \rho_f + (1-\varepsilon_f)\rho_p$), U_0 is the fluid velocity entering through the inlet (dike), and A is the area of active fluid and particles defined below. The mixture viscosity, μ_{mix}, is calculated using the relative viscosity: $\mu_{\mathrm{mix}} = \mu_f \mu_{\mathrm{rel}}$. We use the relationship proposed by *Stickel and Powell* [2005]:

$$\mu_{\mathrm{rel}} = \left(1 - \frac{1-\varepsilon_f}{\varepsilon_{p,\mathrm{max}}}\right)^{-2.5\varepsilon_{p,\mathrm{max}}}, \tag{8}$$

where $\varepsilon_{p,\mathrm{max}}$ is the maximum packing fraction of particles, here chosen as 0.65. We also note that evaluating *Re* at the inlet instead of in the mixing bowl decreases it by a factor of 2.

In single-phase flows, viscous forces prevail when $Re < 1$. The vorticity of large-scale vortices decays by direct viscous stresses over the entire active area. The time scale for mixing is proportional to the rotation time of these large-scale vortices. Their size is constrained by the mixing bowl, they are driven by the thrust coming from the inlet, and the bulk viscosity opposes resistance to their rotation. Dimensional arguments similar to those used in [*Breidenthal et al*., 1990] yield the following characteristic time scale for the viscous regime:

$$t_{\mathrm{mix}-v} = \frac{\sqrt{A}}{U_0} \mu_{\mathrm{rel}}. \tag{9}$$

This time scale can be thought of as the travel time across the active area (A) multiplied by the bulk viscosity contrast of the resident and injected magmas.

In single-phase flows with $Re > 1$, mixing can be simply ascribed to just two scales, the Taylor and the Batchelor layers [*Broadwell and Breidenthal*, 1982; *Broadwell and Mungal*, 1991; *Dimotakis*, 2005]. These are the diffusive spatial scales associated with the largest and the smallest eddies in the flow. As *Re* increases, the sizes of the largest and smallest eddies, as well as their diffusive scales, spread further apart. At a *Re* of

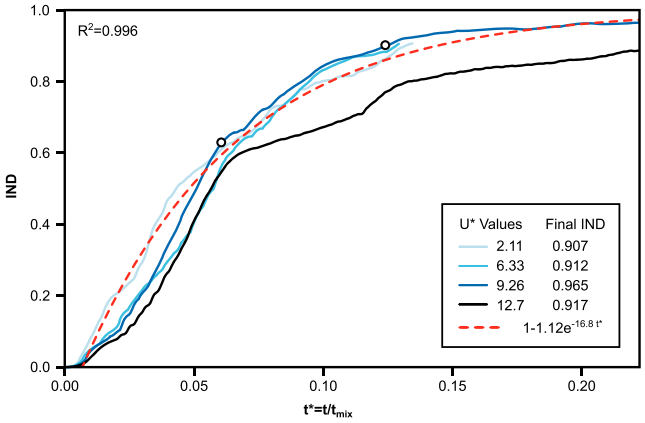

Figure 3. The initial neighbor distance (IND) as a function of dimensionless time (t^*) for four intrusion rates. Time is nondimensionalized by the characteristic mixing time given in equation (9). An exponential curve (red dashed line) is fit to the IND curves for three U^* intrusion rates. The black curve is not included in the fit, see text for discussion. White circles with black outlines display the times and IND values used in Figure 4.

order O(10^3) in a single-phase system, there is an increase in molecular-scale mixing at the mixing transition. The characteristic time scale for mixing in the inertial regime is given as [*Breidenthal et al.*, 1990]

$$t_{\mathrm{mix}-i} = \sqrt{\frac{A^{3/2}\rho_{\mathrm{mix}}}{\rho_f U_0^2 I_w}}. \quad (10)$$

The characteristic mixing time can be thought of as the ratio of the mass of material in the active area to the injection thrust.

Below the mixing transition, the flow is not self-similar and there is no well-defined size for the small-scale vortices, so there is essentially no Batchelor layer. Large-scale motions control mixing in a single- and condensed-phase system and particle dispersion in a two-phase system. Non-Brownian particle dispersion differs from the mixing of a scalar field variable in that it does not depend on a progressive reduction in scale by repeated stretching. Hence, global strain rate may not provide a reliable proxy for the progress of dispersion and multiphase mixing. As a result, mixing and dispersion below the mixing transition do not depend on *Re*.

While *Re* characterizes the dynamics of the motions within the active area, the ratio $t_{\text{mix-}i}/t_{\text{mix-}v}$ characterizes the respective effectiveness of inertial and viscous forces in advancing the actual mixing process by large-scale vortices. *Re* of our simulations straddle unity and $t_{\text{mix-}i}/t_{\text{mix-}v}$ is well below unity. This suggests that while $t_{\text{mix-}v}$ is the most appropriate choice in our runs to calculate the dimensionless times as $t^* = t/t_{\text{mix-}v}$, the role of inertial forces cannot be neglected. This is reflected by the fact that using $t_{\text{mix-}i}$ instead of $t_{\text{mix-}v}$ to calculate t^* collapses the data equally well.

The four simulations shown in Figure 3 have *Re* varying from approximately 0.5 to 5. This variation is associated with the progressive onset of pulsing and active bifurcation of the central chimney (Figure 1b). Pulsing is created by the interplay between the collapse of one margin of the mixing bowl into the base of the fluidized core, followed by the subsequent buildup of pressure from continuously supplied new melt that is then released as a pulse that rises in the central chimney. This pulse undergoes internal circulation and induces small-scale granular vortices described in previous simulations [*Bergantz et al.*, 2015]. However, the appearance of these new, smaller scales of overturn and fluid motion do not seem to produce significant additional crystal separation. It follows that the particle dispersion is essentially independent of *Re* and of $t_{\text{mix-}i}/t_{\text{mix-}v}$, for all $U^* > 1$ given that the range of these two dimensionless quantities in magmatic applications are unlikely to exceed O(10^2) and O(1), respectively. In summary, equation (9) works because the primary contributions to the increasing value of the IND are vertical transport in the chimney, lateral transport at the mush-reservoir interface, and large-scale circulation in the mixing bowl, which are the dominant mechanisms of dispersion. Simply indexing the crystal mixing to the strain history may misrepresent the time scales of crystal separation.

Some care is required to estimate the area term, *A*. Although the mixing bowl (Figure 1) approximates the spatial scale of the initial plastic response of the mush, the entire mixing bowl may not be subsequently fluidized. Hence, the area term must be adjusted to reflect the portion of the mixing bowl that is active or unlocked. Figure 2 provides an empirical estimate of the active area as a function of the input velocity and the bed characteristics

$$\frac{A}{A_{mb}} = 0.187\ln(U^*) + 0.481. \quad (11)$$

The logarithmic relationship chosen for A/A_{mb} and U^* recovers the requirement that the active area of particles approaches zero as the input velocity decreases to zero.

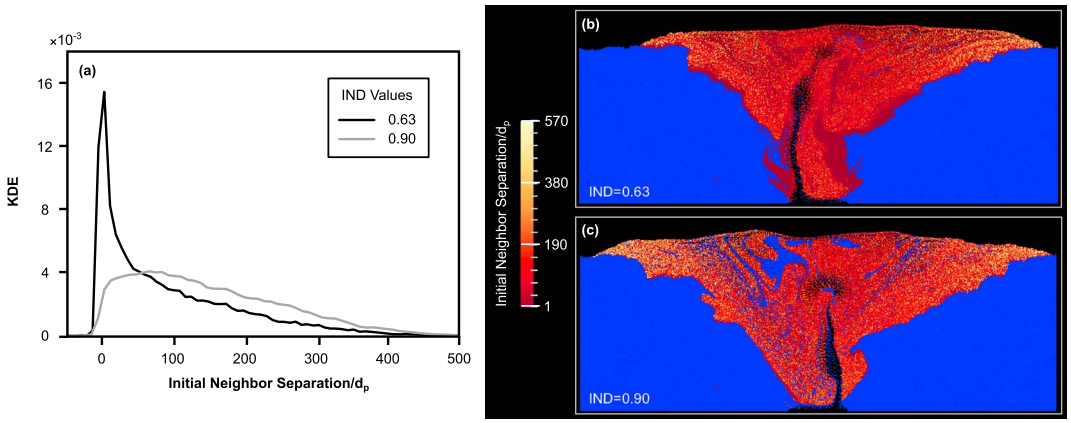

Figure 4. (a) The Kernel density estimation (KDE) of the distribution of distances between crystals and their initial neighbors for the U^* = 9.26 intrusion for IND equal to 0.63 and 0.9. The KDE of the distances at the initial time (IND = 0) has a peak around 1, as many crystals are within one crystal diameter of their initial neighbor. Continued intrusion disperses the crystals, lowering the peak, and extending the tail of the curve to greater particle separation and hence degree of mixing. (b) Initial neighbor distances of particles considered for the IND calculation at an IND of 0.63. (c) Initial neighbor distances of these same particles at an IND of 0.90. Blue regions within the mixing bowl in Figures 4b and 4c are crystals entrained from the walls, and not included in the IND calculation.

We performed four numerical experiments at different values of U^* and calculated the characteristic mixing response using the IND method. All experiments used the same geometry and boundary conditions as shown in Figure 1 but with different values of the input mass flux. The results are shown in Figure 3 where the IND as a function of scaled time is shown. Although the experiments were not terminated at the same value of the IND, they all show an exponential approach to mixing; the three experiments with the lowest U^* exhibiting a statistically significant collapse to a common exponential relationship (Figure 3). The black curve, for a U^* of 12.7, was not included in the exponential relationship as it shows a distinctly different trajectory. Despite having a greater input velocity and hence thrust, the U^* = 12.7 experiment shows a delayed mixing time scale compared to the others. Examination of the simulation reveals that the U^* = 12.7 is so vigorous that some particles in the active region are carried completely out of the mixing bowl, where they are deposited and so removed from any further mixing, yet are still included in the IND calculation. While this process contributes to the global redistribution of crystals, it produces an apparent delay in the progress of mixing as defined by the IND metric.

While the IND provides a single measure for the goodness of mixing of active particles within the entire domain, there will be a distribution around this value, with some portions better mixed than others. We illustrate this in Figure 4a, which is the kernel density estimation, KDE, of the particle pair distances at two points in time. The KDE was constructed using the adaptive kernel density estimator, based on linear diffusion as proposed by *Botev et al.* [2010], which avoids uncertainties associated with KDE bandwidth selection [*Rudge*, 2008; *Vermeesch*, 2012]. Two curves are shown for the simulation with U^* = 9.26 representing IND values of 0.63 and 0.90, which are also shown as small circles in Figure 3. Figures 4b and 4c illustrate how the particle spacing distribution changes as a function of the IND, with a noticeable change going from an IND of 0.63 to 0.90. The KDE and particle spacing distribution for IND equal to 0.63 (Figures 4a and 4b) show that a significant number of particles are still in close proximity to their initial neighbor. A practical implication of this is that it would take numerous geological samples to adequately characterize the diversity of mixing conditions that coexisted during the open-system event. When the IND equals 0.9, Figures 4a and 4c show that the distance between initial particle pairs is distributed more uniformly and is much greater. Nonetheless, even at an IND of 0.9, some elements of the system remain relatively unmixed.

4.2. Applications to Natural Systems

Here we exemplify the application of the IND framework to a natural example at two values of the input mass flux. Consider a 500 m thick crystal mush, composed of basaltic melt and olivine crystals, as might be found in an ocean island, mid-ocean ridge or a composite system like Iceland. We use a melt viscosity and density of

2 Pa s and 2650 kg/m^3, respectively. The crystal density is 3300 kg/m^3 and diameters are 0.002 m, creating an overall mush porosity of 0.4. If a crystal-free basaltic intrusion enters the mush from a meter-wide dike, the minimum fluidization velocity of the system is 0.005 m/s. Using the relationships described above, an intrusion entering at $U^* = 9.26$ would fluidize a volume of ~130,000 m^3 per meter of dike length normal to the mixing bowl span. The crystals in the active area would achieve an IND mixing value of 0.9 after 20 h of sustained intrusion, based on the viscous time scale given in equation (9). If the inertial time scale is used, it increases this duration by a factor of 8. The amount of new melt that would have come into the system is ~3400 m^3, which is ~2.6% of the volume activated by the intrusion. This is a mass flux rate of approximately 0.0015 km^3/yr, roughly two orders of magnitude lower than the long-term rate calculated for the Kilauea system [*Poland et al*., 2012] and about one order of magnitude lower than that estimated for the Hekla volcano in south Iceland [*Geirsson et al*., 2012]. If the input dike length is greater, the corresponding input velocity will be lower to match the same mass flux, and the $U^* = 2.11$ may provide a better estimate of the input velocity and fluidization potential. Under these conditions it will take approximately 73 h of continuous magma input to reach an IND of 0.9. Given the geophysically constrained estimates of mass flux into basaltic systems, we conclude that the active crystal cargo of a natural basaltic crystal mush will likely be well mixed during reintrusion events on a time scale of days to tens of days [*Costa et al*., 2010; *Kahl et al*., 2015].

5. Summary and Conclusions

Crystal mixing in basaltic magma mushes was quantified by introduction of the initial neighbor distance (IND) method. The IND method satisfies many of the criteria for a robust metric of mixing and provides a global measure of the loss of spatial correlation from an initial distribution of crystals in the crystal-rich mush. The IND was applied to a model open-system reintrusion event in a basaltic magma chamber, and two characteristic mixing time scales were introduced that allow for the estimation of the time to mixing under a variety of geologically relevant conditions. A kernel distribution estimation was employed to illustrate the distribution of local crystal segregation scales around the global IND value. Application to natural basaltic systems reveals that mixing of a basaltic crystal mush can occur within days with geologically inferred magma intrusion rates.

Acknowledgments
Financial support was provided by National Science Foundation grants EAR-1049884 and EAR-1447266 to G.W.B. and DGE-1256082 to J.M.S. A grant from Labex OSUG@2020 (ANR1O LABX56) partly supported A.B. Access to computational facilities was provided by grant TG-EAR140013 to G.W.B. from the NSF-funded XSEDE consortium. David Neave and Marie Edmunds are thanked for their careful and constructive comments.

References

Bec, J., A. Celani, M. Cencini, and S. Musacchio (2005), Clustering and collisions of heavy particles in random smooth flows, *Phys. Fluids*, *17*(7), doi:10.1063/1.1940367.

Bergantz, G. W. (2000), On the dynamics of magma mixing by reintrusion: Implications for pluton assembly processes, *J. Struct. Geol.*, *22*(9), 1297–1309.

Bergantz, G. W., J. M. Schleicher, and A. Burgisser (2015), Open-system dynamics and mixing in magma mushes, *Nat. Geosci.*, *8*(10), 793–796, doi:10.1038/ngeo2534.

Botev, Z. I., J. F. Grotowski, and D. P. Kroese (2010), Kernel density estimation via diffusion, *Ann. Stat.*, *38*(5), 2916–2957, doi:10.2307/29765251.

Bouzid, M., M. Trulsson, P. Claudin, E. Clément, and B. Andreotti (2013), Nonlocal rheology of granular flows across yield conditions, *Phys. Rev. Lett.*, *111*(23), 238301.

Breidenthal, R. E., V. R. Buonadonna, and M. F. Weisbach (1990), Molecular mixing via jets in confined volumes, *J. Fluid Mech.*, *219*, 531–544.

Broadwell, J. E., and M. G. Mungal (1991), Large-scale structures and molecular mixing, *Phys. Fluids A*, *3*, 1193–1206.

Broadwell, J. E., and R. E. Breidenthal (1982), A simple model of mixing and chemical reaction in a turbulent shear layer, *J. Fluid Mech.*, *125*, 397–410, doi:10.1017/S0022112082003401.

Charlier, B. L. A., O. Bachmann, J. P. Davidson, M. A. Dungan, and D. J. Morgan (2007), The upper crustal evolution of a large silicic magma body: Evidence from crystal-scale Rb-Sr isotopic heterogeneities in the Fish Canyon Magmatic System, Colorado, *J. Petrol.*, *48*(10), 1875–1894, doi:10.1093/petrology/egm043.

Coltice, N., and J. Schmalzl (2006), Mixing times in the mantle of the early Earth derived from 2-D and 3-D numerical simulations of convection, *Geophys. Res. Lett.*, *33*, L23304, doi:10.1029/2006GL027707.

Costa, F., L. A. Coogan, and S. Chakraborty (2010), The time scales of magma mixing and mingling involving primitive melts and melt-mush interaction at mid-ocean ridges, *Contrib. Mineral. Petrol.*, *159*, 371–387.

Cui, X., J. Li, A. Chan, and D. Chapman (2014), Coupled DEM–LBM simulation of internal fluidisation induced by a leaking pipe, *Powder Technol.*, *254*, 299–306, doi:10.1016/j.powtec.2014.01.048.

Davidson, J. P., J. M. Hora, J. M. Garrison, and M. A. Dungan (2005), Crustal forensics in arc magmas, *J. Volcanol. Geotherm. Res.*, *140*, 157–170.

Davidson, J. P., D. J. Morgan, B. L. A. Charlier, R. Harlou, and J. M. Hora (2007), Microsampling and isotopic analysis of igneous rocks: Implications for the study of magmatic systems, *Annu. Rev. Earth Planet. Sci.*, *35*(1), 273–311, doi:10.1146/annurev.earth.35.031306.140211.

Deen, N. G., G. Willem, G. Sander, and J. A. M. Kuipers (2010), Numerical analysis of solids mixing in pressurized fluidized beds, *Ind. Eng. Chem. Res.*, *49*(11), 5246–5253, doi:10.1021/ie9014843.

Dimotakis, P. E. (2005), Turbulent mixing, *Annu. Rev. Fluid Mech.*, *37*, 329–356, doi:10.1146/annurev.fluid.36.050802.122015.

Doucet, J., F. Bertrand, and J. Chaouki (2008), A measure of mixing from Lagrangian tracking and its application to granular and fluid flow systems, *Chem. Eng. Res. Des.*, *86*(12), 1313–1321, doi:10.1016/j.cherd.2008.09.003.

Farnetani, C. G., and H. Samuel (2003), Lagrangian structures and stirring in the Earth's mantle, *Earth Planet. Sci. Lett.*, *206*(3–4), 335–348, doi:10.1016/S0012-821X(02)01085-3.

Ferrachat, S., and Y. Ricard (1998), Regular vs. chaotic mantle mixing, *Earth Planet. Sci. Lett.*, *155*(1–2), 75–86, doi:10.1016/S0012-821X(97)00200-8.

Geirsson, H., P. LaFemina, T. Árnadóttir, E. Sturkell, F. Sigmundsson, M. Travis, P. Schmidt, B. Lund, S. Hreinsdóttir, and R. Bennett (2012), Volcano deformation at active plate boundaries: Deep magma accumulation at Hekla volcano and plate boundary deformation in south Iceland, *J. Geophys. Res.*, *117*, B11409, doi:10.1029/2012JB009400.

Ginibre, C., G. Wörner, and A. Kronz (2007), Crystal zoning as an archive for magma evolution, *Elements*, *3*(4), 261–266, doi:10.2113/gselements.3.4.261.

Guazzelli, E., and J. F. Morris (2012), *A Physical Introduction to Suspension Dynamics*, 229 pp., Cambridge Univ. Press, New York.

Jellinek, A. M., R. C. Kerr, and R. W. Griffiths (1999), Mixing and compositional stratification produced by natural convection: 1. Experiments and their application to Earth's core and mantle, *J. Geophys. Res.*, *104*(B4), 7183–7201, doi:10.1029/1998JB900116.

Kahl, M., S. Chakraborty, F. Costa, and M. Pompilio (2011), Dynamic plumbing system beneath volcanoes revealed by kinetic modeling, and the connection to monitoring data: An example from Mt. Etna, *Earth Planet. Sci. Lett.*, *308*(1–2), 11–22, doi:10.1016/j.epsl.2011.05.008.

Kahl, M., S. Chakraborty, M. Pompilio, and F. Costa (2015), Constraints on the nature and evolution of the magma plumbing system of Mt. Etna volcano (1991–2008) from a combined thermodynamic and kinetic modelling of the compositional record of minerals, *J. Petrol.*, *56*, 2025–2068, doi:10.1093/petrology/egv063.

Kellogg, L. H., and D. L. Turcotte (1990), Mixing and the distribution of heterogeneities in a chaotically convecting mantle, *J. Geophys. Res.*, *95*(B1), 421–432, doi:10.1029/JB095iB01p00421.

Klemetti, E. W., and M. A. Clynne (2014), Localized rejuvenation of a crystal mush recorded in zircon temporal and compositional variation at the Lassen Volcanic Center, Northern California, *PLoS One*, *9*(12), e113157, doi:10.1371/journal.pone.0113157.

Laumonier, M., B. Scaillet, L. Arbaret, and R. Champallier (2014), Experimental simulation of magma mixing at high pressure, *Lithos*, *196–197*, 281–300, doi:10.1016/j.lithos.2014.02.016.

Lemaître, A., J.-N. Roux, and F. Chevoir (2009), What do dry granular flows tell us about dense non-Brownian suspension rheology?, *Rheol. Acta*, *48*(8), 925–942, doi:10.1007/s00397-009-0379-3.

Martin, V. M., J. Davidson, D. Morgan, and D. A. Jerram (2010), Using the Sr isotope compositions of feldspars and glass to distinguish magma system components and dynamics, *Geology*, *38*(6), 539–542, doi:10.1130/g30758.1.

Marzougui, D., B. Chareyre, and J. Chauchat (2015), Microscopic origins of shear stress in dense fluid–grain mixtures, *Granular Matter*, *17*(3), 297–309, doi:10.1007/s10035-015-0560-6.

Mutabaruka, P., J.-Y. Delenne, K. Soga, and F. Radjai (2014), Initiation of immersed granular avalanches, *Phys. Rev. E*, *89*(5), 052203.

Ness, C., and J. Sun (2015), Flow regime transitions in dense non-Brownian suspensions: Rheology, microstructural characterization, and constitutive modeling, *Phys. Rev. E*, *91*(1), 012201.

Oldenburg, C. M., F. J. Spera, D. A. Yuen, and G. Sewell (1989), Dynamic mixing in magma bodies: Theory, simulations and implications, *J. Geophys. Res.*, *94*, 9215–9236, doi:10.1029/JB094iB07p09215.

Passmore, E., J. Maclennan, G. Fitton, and T. Thordarson (2012), Mush disaggregation in basaltic magma chambers: Evidence from the AD 1783 Laki eruption, *J. Petrol.*, *53*(12), 2593–2623, doi:10.1093/petrology/egs061.

Perugini, D., and G. Poli (2012), The mixing of magmas in plutonic and volcanic environments: Analogies and differences, *Lithos*, *153*, 261–277, doi:10.1016/j.lithos.2012.02.002.

Perugini, D., C. P. De Campos, W. Ertel-Ingrisch, and D. B. Dingwell (2012), The space and time complexity of chaotic mixing of silicate melts: Implications for igneous petrology, *Lithos*, *155*, 326–340, doi:10.1016/j.lithos.2012.09.010.

Poland, M. P., A. Miklius, A. Jeff Sutton, and C. R. Thornber (2012), A mantle-driven surge in magma supply to Kilauea Volcano during 2003–2007, *Nat. Geosci.*, *5*(4), 295–300.

Poux, M., P. Fayolle, J. Bertrand, D. Bridoux, and J. Bousquet (1991), Powder mixing: Some practical rules applied to agitated systems, *Powder Technol.*, *68*(3), 213–234, doi:10.1016/0032-5910(91)80047-M.

Rudge, J. F. (2008), Finding peaks in geochemical distributions: A re-examination of the helium-continental crust correlation, *Earth Planet. Sci. Lett.*, *274*(1–2), 179–188, doi:10.1016/j.epsl.2008.07.021.

Ruprecht, P., G. W. Bergantz, K. M. Cooper, and W. Hildreth (2012), The crustal magma storage system of Volcán Quizapu, Chile, and the effects of magma mixing on magma diversity, *J. Petrol.*, *53*(4), 801–840, doi:10.1093/petrology/egs002.

Sato, E., and H. Sato (2009), Study of effect of magma pocket on mixing of two magmas with different viscosities and densities by analogue experiments, *J. Volcanol. Geotherm. Res.*, *181*(1–2), 115–123, doi:10.1016/j.jvolgeores.2009.01.005.

Stickel, J. J., and R. L. Powell (2005), Fluid mechanics and rheology of dense suspensions, *in Annu. Rev. Fluid Mech.*, *37*, 129–149.

Tackley, P. J., and S. D. King (2003), Testing the tracer ratio method for modeling active compositional fields in mantle convection simulations, *Geochem. Geophys. Geosyst.*, *4*(4), 8302, doi:10.1029/2001GC000214.

Turner, J. S., and I. H. Campbell (1986), Convection and mixing in magma chambers, *Earth Sci. Rev.*, *23*, 255–352.

van Keken, P., and S. Zhong (1999), Mixing in a 3D spherical model of present-day mantle convection, *Earth Planet. Sci. Lett.*, *171*(4), 533–547, doi:10.1016/S0012-821X(99)00181-8.

Vermeesch, P. (2012), On the visualisation of detrital age distributions, *Chem. Geol.*, *312–313*, 190–194, doi:10.1016/j.chemgeo.2012.04.021.

Wallace, G. S., and G. W. Bergantz (2005), Reconciling heterogeneity in crystal zoning data: An application of shared characteristic diagrams at Chaos Crags, Lassen Volcanic Center, California, *Contrib. Mineral. Petrol.*, *149*, 98–112.